Simultaneous removal of NO and Hg^0 using Fe and Co co-doped Mn-Ce/TiO_2 catalysts

Boxiong Shen[a,*], Shaowen Zhu[b], Xiao Zhang[a], Guilong Chi[a], Dipesh Patel[c], Meng Si[a], Chunfei Wu[a,c,*]

[a] *School of Energy & Environmental Engineering, Hebei University of Technology, Tianjin, China*
[b] *College of Environmental Science & Engineering, Nankai University, Tianjin, China*
[c] *School of Engineering and Computer Science, University of Hull, Hull, HU6 7RX, UK*

*Corresponding author: Professor Boxiong Shen.
E-mail: shenbx@hebut.edu.cn Tel:86-22-60435784

Abstract: Fe and Co co-doped Mn-Ce/TiO_2 (MCT) catalysts were investigated for the simultaneous removal of nitric oxide (NO) and elemental mercury (Hg^0) at reaction temperature lower than 200 °C. The catalysts were characterized by Brunauer–Emmett–Teller (BET), temperature program reduction (TPR), scanning electron microscope (SEM), x-ray diffraction (XRD) and x-ray photoelectron spectroscopy (XPS) analysis. The experimental results showed that the co-doped 2Fe4Co-MCT catalyst exhibited better performance for the simultaneous removal of NO and Hg^0 compared to Fe or Co doped catalysts. This could be due to higher BET surface area and better redox property of 2Fe4Co-MCT catalyst. In addition, we propose that chemisorbed O_2 played a dominant role in selective catalytic reduction (SCR) of NO while lattice O_2 played a key role in Hg^0 oxidation. The results also indicate that the introduction of Fe species enhanced the activity of SCR, whereas the introduction of Co species enhanced the oxidation of Hg^0. The synergistic effect of Fe and Co species in the 2Fe4Co-MCT catalyst are also suggested to be an important mechanism for simultaneously removing NO and Hg^0.

Keywords: Simultaneous removal; Nitric oxide; Elemental mercury; Fe-Co

1. Introduction

Mercury emitted from coal-fired power plants, cement kiln and solid waste incineration units normally has three forms: 1) elemental mercury (Hg^0), 2) Oxidized mercury (Hg^{2+}) and 3) Particle-bond mercury (Hg^p) [1, 2]. Hg^p can be easily removed by dust removal systems such as electrostatic precipitator or bag-type dust remover. Hg^{2+} is soluble in water and can be easily captured by wet flue gas desulfurization (WFGD) scrubber. However, Hg^0 is volatile and insoluble in water Common air pollution control devices (APCDs) is normally used to remove mercury. The overall efficiency of mercury removal in APCDs ranges from 43.8% to 94.9%, depending on the form of mercury and the operating conditions [3]. To meet the increasingly strict environmental standards of mercury control, it is necessary to develop an enhanced or supplementary process to increase the removal of mercury.

There are two key approaches to enhance the removal of mercury from flue gas. The first method is to absorb mercury using adsorbents. The other method is to oxidize Hg^0 to Hg^{2+} which can then be captured by downstream WFGD. The injection of powder carbon materials has been commercially applied for the removal of mercury from flue gas. To enhance the chemisorption of Hg^0 on the surface of carbon-based adsorbents, various reagents have been used to modify these carbonaceous adsorbents. For example, activated carbons were treated by acids including H_2SO_4, HNO_3 or $HClO_4$ to enhance the removal of Hg^0, due to the formation of oxygen-containing (C-O) or chlorine-containing groups (C-Cl) on the surface of the adsorbents [4]. Various kinds of chlorides such as $ZnCl_2$ [5-8], $FeCl_3$ [7] and NH_4Cl [8] were used as predecessors to modify

carbonaceous adsorbents to improve the efficiency of mercury removal. The chemisorption between carbonaceous materials and Hg^0 was enhanced after the modification of adsorbent such as sulfur treatment [9] and the addition of CeO_2 [7, 10] However, using sorbent to remove Hg^0 has some drawbacks [11]: 1) a large amount of sorbent is required for the adsorption of Hg^0 indicating the high cost of sorbent use; 2) the disposal challenges of the exhaust sorbents mixed with fly ash.

In flue gas, the oxidation of Hg^0 to Hg^{2+} could be obtained using oxidants such as a mixture of urea and $KMnO_4$ solution [12], $NaClO_2$ solution [13-15], H_2O_2 solution [16, 17], K_2FeO_4 [18], and Fenton reagent [19, 20]. However, the corrosive nature of the oxidants limits the deployment of such technology, even though the direct oxidation of Hg^0 using oxidants has higher removal efficiency. Therefore, the oxidation of Hg^0 by catalyst seems to be a preferable alternative because it has a low secondary pollution.

$CePO_4$ catalyst was employed to capture elemental mercury and showed much better performance in Hg^0 removal compared with a commercial SCR catalyst [21]. The $CePO_4$ catalyst promoted the formation of nitrogen dioxide (NO_2) from NO oxidation. And NO_2 was effective to react with Hg^0 ad-species (e.g., Hg_2O) [21]. $LaMnO_3$ perovskite oxide was chosen to remove Hg^0. The results indicated that mercury primarily existed as Hg–O, and the used $LaMnO_3$ catalyst can be regenerated using thermal desorption [22]. $La_{1-X}Sr_XMnO_3$ have been investigated to oxidize Hg^0 at low temperature of 100-200 °C [23]. Due to the low cost and the excellent performance for mercury oxidation, TiO_2-supported catalysts have been widely investigated to remove mercury including molybdenum (Mo) and ruthenium (Ru) modified V_2O_5-WO_3/TiO_2

[24], Ce-doped V_2O_5-CeO_2/TiO_2 [25], nanosized V_2O_5/TiO_2 [26] and MnO_X-CeO_2/TiO_2 [27, 28].

In addition, more strict regulations are applied to reduce the emission of other pollutants (e.g. NOx) in coal-fired power plants. At the moment, medium temperature selective catalytic reduction (SCR, around 350 °C) is commercially available for the removal of NOx in coal-fired power plants. However, the installation of medium temperature SCR system needs a large space which should be located before the removal of particulate matter. Installing low temperature SCR system (less than 200 °C) could solve the problem, as the SCR catalyst is unlikely to be deactivated compared with the catalyst for medium-temperature SCR. Therefore, the simultaneous removal of NO and Hg^0 by the oxidation at low temperature SCR system employing various catalysts has been proposed and investigated [29, 30].

In terms of low temperature SCR, MnOx based catalyst has been widely studied [31-33]. Ji et al. [34] found that MnOx/TiO_2 catalyst could achieve high efficiency for the removal of NO at low temperature. Similarly, CeO_2 has a large capacity of oxygen storage and has been extensively used as a catalyst for low temperature SCR [35, 36]. Our previous study showed that Ce was an efficient promoter in low temperature SCR [37]. Additionally, interactions between CeO_2 and MnOx were found to be crucial to improve SCR performance as reported by Qi et al. [38].

Therefore, a catalyst containing Mn, Ce and TiO_2 seems to be effective for the simultaneous removal of NOx and Hg^0. In addition, Fe and Co have been widely examined as active sites for SCR process. Qi et al. [39] found that the addition of iron oxide not only increased the NO conversion but also increased the resistance to H_2O

and SO_2. Shen et al. [40] also reported that the doping of iron enhanced the dispersion of Mn and Ce on the surface of the catalyst. The presence of Fe^{3+} active sites could promote the oxidation of NO to NO_2 by O_2 resulting in an improvement of NOx reduction in the NH_3-SCR process [41]. The formation of Co-Mn oxides was found to be important in SCR process [42, 43]. In addition, Co oxides have been reported to efficiently absorb active oxygen by generating oxygen vacancy derived from the conversion of Co^{3+}/Co^{2+} [25, 44]. The addition of Co into nanoporous nickel phosphate has been reported to enhance the catalytic efficiency of NOx reduction [45, 46]. However, to the best of our knowledge, the co-doping of Fe and Co in Mn-Ce/TiO_2 catalyst for the simultaneous removal of NO and mercury has not been reported in literature. In this study, a series of Mn-Ce/TiO_2 catalysts modified with Fe and Co have been investigated aiming to enhance the simultaneous removal of NO and Hg^0 at low temperature.

2. Experimental

2.1. Catalyst preparation

All catalysts were prepared by wet impregnation method. An appropriate proportion of precursors (the nitrate of Mn, Ce, Fe and Co) were dissolved in excess deionized water and a corresponding amount of TiO_2 was added to the solution. The molar ratio of (Fe+Co): Mn: Ce: TiO_2 was 0.075:0.12:0.024:1. The total moles of Fe and Co were kept constant while Fe/Co ratios were changed. The precursors were mixed using a water bath with continuous stirring at 80 °C. The samples were then dried in an oven at 120 °C overnight and then calcined in an electric furnace at 500 °C for 4 h. The catalysts were ground and sieved to granules (40-80 mesh) for further characterizations and experimental uses. Mn-Ce/TiO_2 catalyst is indicated as MCT. MCT catalyst with Fe addition is assigned as 6Fe-MCT. In addition, MCT catalyst with Co addition is

assigned as 6Co-MCT. And 2Fe4Co-MCT indicates the MCT catalyst having a Fe/Co molar ratio of 2:4.

2.2. Catalytic activity test

The catalytic activities were carried out in a fixed-bed reactor as shown in Fig. 1. The flue gases including NO, NH_3, O_2 and N_2 were obtained from the compressed gas tanks and were adjusted by mass flow controllers (MFC). A mercury permeation tube (VICI Metronics Inc., USA) ("U" type tube) was used to provide a uniform and stable release of elemental mercury vapor by the carrier gas. The "U" type tube was dipped into a water bath. The concentration of Hg^0 entering the reactor was controlled by regulating the temperature of the water bath and the flow rate of the carrier gas. All gases were converged and blended in a mixer first and then fed to the reactor. NaOH solution was used to remove the residual NO and NH_3, while a silica gel was used to eliminate the effect of water vapor. The total gas flow rate was maintained at 1500 mL min^{-1} with a gas hourly space velocity of 30000 h^{-1}, corresponding to 3 ml catalyst was used in each experiment. The concentrations of NO and Hg^0 at the inlet and outlet of the reactor were monitored and measured by a flue gas analyzer (KM900, Kane International Ltd, UK) and a Hg analyzer (MI VM-3000, Germany), respectively.

The removal efficiency or conversion of NO (E_{NO}) and Hg^0 (E_{Hg^0}) was defined by Eqs. 1 and 2, respectively. In equations (1) and (2), NO_{in} and NO_{out} represent the NO concentrations at the inlet and outlet of the reactor, and Hg^0_{in} and Hg^0_{out} represent the Hg^0 concentrations at the inlet and outlet of the reactor, respectively.

$$\%E_{NO} = \frac{NO_{in} - NO_{out}}{NO_{in}} \text{ x } 100 \quad (1)$$

$$\%E_{Hg^0} = \frac{Hg^0{}_{in} - Hg^0{}_{out}}{Hg^0{}_{in}} \text{ x } 100 \quad (2)$$

To investigate the performance of catalysts for the simultaneous removal of NO and Hg^0, a series of experiments were carried out. The experimental conditions are summarized in Table 1. Set A experiments were conducted to compare the performance of the Fe/Co co-doped catalyst with only Fe or Co doped Mn-Ce/TiO_2 (MCT) catalyst for simultaneously removing NO and Hg^0. Set B and Set C experiments were conducted to investigate the interaction between the removal of NO and the reduction Hg^0 at different temperature using the 2Fe4Co-MCT catalyst. Set D experiments were set up to investigate the influence of flue gas components on the removal of Hg^0 in the presence of the 2Fe4Co-MCT catalyst.

2.3. Catalyst characterization

BET surface area, pore volume and pore size of the catalysts were determined by nitrogen adsorption/desorption at –196 °C using a Micromeritics Accelerated Surface Area and Porosimetry (ASAP) 2020 instrument. Scanning electron microscopy (SEM) was performed using a scanning electron microscope (SS-550, Shimadzu, Japan). Powder x-ray diffraction (XRD) measurement was used to identify the crystal structures of the catalysts with Rigaku D/Max 2500 system using Cu Kα radiation (40 kV, 100 mA) (Rigaku Corporation, Japan).

Temperature programmed reduction of H_2 (H_2-TPR) was conducted on a PCA-1200 chemisorption analyzer using 100 mg of catalysts to analyze the redox properties of the catalysts. Prior to the TPR experiment, the catalyst samples were dried in a N_2 flow (30 mL min^{-1}) for 2 h at 200 °C. After drying the catalyst samples, the reduction experiment was performed in a mixture gas (30 mL min^{-1}) containing 5% H_2 and balance N_2 from 100–900 °C with a heating rate of 10 °C min^{-1}. The concentration of H_2 from the outlet of the system was monitored by a thermal conductivity detector (TCD). The surface atomic state of the fresh and used 2Fe4Co-MCT catalysts was investigated by x-ray photoelectron spectroscopy (XPS) using Al-Kα radiation (hν = 1486.6 eV) monochromate, calibrated using the C1s (284.6ev) as an internal reference.

3. Result and discussion

3.1. Catalytic activity

Fig. 2 shows the results of the simultaneous removal of NO and Hg^0 for the Set A experiments. From Fig. 2(a), the efficiency of NO removal was increased when the temperature was increased from 100 to 200 °C. Fig. 2(b) shows the efficiency of Hg^0 removal over the catalyst in the presence of 500 ppm NO and 500 ppm NH_3 (SCR conditions). The removal efficiency of Hg^0 increased between 100 and 150 °C. However, the removal efficiency of Hg^0 was decreased as the reaction temperature increased from 150 to 300 °C. A higher temperature seems to be unfavorable for the removal of Hg^0. In particular when the reaction temperature was higher than 250 °C. Nevertheless, the 2Fe4Co-MCT catalyst exhibited the highest efficiency of the simultaneous removal of NO and Hg^0 compared with the Fe or Co doped catalysts.

To further understand the effect of Hg^0 on NO removal by the 2Fe4Co-MCT catalyst, a series of experiments were carried out (as Set B listed in Table 1). As shown in Fig. 2(c), the efficiency of NO removal was gradually increased between 100 and 200 °C and then decreased with an increase of the reaction temperature from 200 to 300 °C. This is true irrespective of the experiments carried out in the absence or in the presence of Hg^0. The maximum NO removal efficiency was achieved at 200 °C. At temperature over 200 °C, the introduction of Hg^0 had little effect on the removal of NO. It is suggested that the concentration of Hg^0 was very small compared to the concentration of NO in the flue gas. The inhibition of NO removal by Hg^0 at temperature lower than 200 °C could be due to the greater adsorption of mercury species on the catalytic surface at low temperature, thereby reducing the availability of active sites for SCR reactions.

To investigate the effect of SCR conditions on the removal of Hg^0, the removal of Hg^0 was investigated with or without the addition of NO and NH_3 at temperature between 100 and 300 °C. As shown in Fig. 2(d) (experiments as Set C), the presence of NO and NH_3 (SCR conditions) had a negative influence on the removal of Hg^0. For example, the efficiency of Hg^0 removal was reduced significantly from 92% at 100 °C to 55% at 250 °C, when the SCR condition was used in the experiment. This could be due to that NH_3 species significantly occupied the active sites on the surface of the catalyst. Therefore, there were less surface areas for Hg^0 adsorption [27, 47].

The effect of the presence of other flue gas components on the removal of Hg^0 was studied in Set D experiment. As shown in Fig. 2(e), the outlet concentration of Hg^0 was increased rapidly and almost reached a breakthrough after 12 h when only N_2 was used

as carrier gas. With the addition of O_2, the removal efficiency of Hg^0 was enhanced significantly, as the outlet concentration of Hg^0 was reduced from 28 μg m^{-3} to around 7.5 μg m^{-3}. Therefore, the oxidation of Hg^0 on the surface of the catalyst was enhanced in the presence of O_2. The addition of 500 ppm NO showed little effect on the removal of Hg^0, indicating that the addition of NO was not the main factor affecting Hg^0 removal. On the contrary, NO was reported to promote the oxidation of Hg^0 in the presence of a Ce-MnO_x/Ti-PILCs catalyst [40]. From Fig. 2(e), the addition of 500 ppm NH_3 (without NO in flue gas) inhibited the removal of Hg^0, demonstrating that NH_3 was the main component competing for active sites with Hg^0 on the surface of the catalyst. This observation is consistent with other reports regarding the competitive adsorption of NH_3 with Hg^0 [48, 49].

3.2. Catalyst characterizations

The physical properties of the produced Mn-Ce/TiO_2 (MCT) catalysts are listed in Table 2. The BET surface area of the Mn-Ce/TiO_2 was 17.06 m^2 g^{-1}. Among the three modified catalysts, the 2Fe4Co-MCT catalyst achieved the highest BET surface area of 23.02 m^2 g^{-1}, while the BET surface area of the 6Fe-Mn-Ce/TiO_2 catalyst and the 6Co-Mn-Ce/TiO_2 catalyst were 22.25 m^2 g^{-1} and 16.37 m^2 g^{-1}, respectively. The BET surfaces area, pore volume and pore size of catalysts all increased after the doping of Fe and/or Co. The increase of BET surfaces area and porosity is beneficial for the transfer of gas molecules in the interspace of the catalysts. Enhanced gas transfer in the catalyst is favorable for SCR reactions and the removal of mercury [50].

SEM pictures of the fresh catalysts are shown in Fig. 3. The agglomeration of particles

is observed on the surface of the fresh MCT catalyst. Particle agglomeration is reduced with the addition of Fe or Co. The 2Fe4Co-MCT catalyst has uniform distribution of metal particles suggesting that the co-addition of Fe and Co enhanced the distribution of metal particles on the surface of the catalyst.

The XRD patterns of the MCT, the 6Fe-MCT, the 6Co-MCT, the 2Fe4Co-MCT and anatase TiO_2 catalysts are shown in Fig. 4. All peaks were attributed to anatase TiO_2 and peaks related to the oxides of Fe, Co, Mn and Ce could be hardly found. This might be due to the concentrations of metal oxides were low or the size of crystals presented on the surfaces of TiO_2 was too small to be detected by XRD.

The redox properties of the fresh catalysts were studied by H_2-TPR analysis. The results are shown in Fig. 5. A broad peak between 250 and 500 °C and one peak near 550 °C could be observed for the Mn-Ce/TiO_2 catalyst. The first reduction peak around 360 °C could be assigned to the reduction of MnO_2 to Mn_2O_3, while the reduction peak at 460 °C was possibly attributed to the stepwise reduction of Mn_2O_3 to MnO [25, 51, 52]. The peak occurred near 550 °C was likely due to the stepwise reduction of Ce^{4+} to Ce^{3+} [43]. Fig. 5(b) shows the H_2-TPR profile of the 6Fe-Mn-Ce/TiO_2. In addition to similar reduction peaks to the Mn-Ce/TiO_2 at temperature between 250 and 500 °C, some small broad reduction peaks between 550 and 800 °C are found for the 6Fe-Mn-Ce/TiO_2 catalyst, due to the addition of Fe species. The reduction peaks around 605 and 695 °C could be ascribed to the stepwise reduction process of $Fe_3O_4 \rightarrow FeO \rightarrow Fe$ [51, 53, 54]. The width and intensity of these peaks around 250–550 °C increased, especially at temperature near 342 and 486 °C. The peaks at 342 and 376 °C could be attributed to

the simultaneous reduction of MnO_2 to Mn_2O_3 and Fe_2O_3 to Fe_3O_4 [51, 53, 55], while the reduction peak at 486 °C may be assigned to the coinstantaneous reduction of Mn_2O_3 and CeO_2 [51, 55].

Fig. 5(c) shows the H_2-TPR profile of the 6Co-Mn-Ce/TiO_2 catalyst. Similar to the Mn-Ce/TiO_2, three reduction peaks between 250 and 500 °C and two new broad peaks above 500 °C are observed. The interaction between Co and Mn to form compound has been reported [25, 56, 57]. The three reduction peaks at 317 °C, 362 °C and 430 °C were suggested to be the combined reduction of Co_3O_4, MnO_x, $CoMnO_3$ and $CoMn_2O_4$ [25, 56]. The peaks around 547 and 603 °C may be attributed to the simultaneous reduction of Ce^{4+} to Ce^{3+} and CoO to Co [25, 43]. Fig. 5(d) shows the reduction of Fe and Co co-doped catalysts. Several key reduction peaks around 349 °C, 414 °C, 457 °C and 593 °C were observed for the TPR of the 2Fe4Co-Mn-Ce/TiO_2 catalyst. The reduction around 349 °C, 457 °C and 593 °C are similar to the reduction of the MCT catalyst (Fig. 5(a)). These peaks are assigned to the reduction of MnO_2 to Mn_2O_3, the stepwise reduction of Mn_2O_3 to MnO, and the stepwise reduction of Ce^{4+} to Ce^{3+}, respectively. The reduction around 312 °C, 349°C and 424 °C for the 2Fe4Co-Mn-Ce/TiO_2 catalyst (Fig.5(d)) is related to the combined reduction of Co_3O_4, MnO_x, $CoMnO_3$ and $CoMn_2O_4$ as indicated in the reduction of the 6Co-Mn-Ce/TiO_2 catlayst (Fig. 5(c)). The reduction around 717 °C could be assigned to the reduction of Fe species presented in the 2Fe4Co-MCT catalyst.

The intensity of the peaks in Fig. 5(d) for the 2Fe4Co-MCT, especially at the temperature between 500 and 700 °C, was stronger and sharper compared with the

catalyst doped with either Fe or Co. Therefore, the 2Fe4Co-MCT catalyst has a higher oxidation state as more H_2 was consumed at this temperature range. From the H_2-TPR results, the intensities and areas of the reduction curves assigned to the modified catalysts were increased compared to the MCT catalyst. Therefore, the catalysts doped with Fe or Co might have higher redox properties, especially for the 2Fe4Co-MCT catalyst. The higher redox property is favorable for the removal of NO and Hg^0.

3.3. XPS analysis of 2Fe4Co-MCT catalysts

To reveal the mechanisms of simultaneous removal of NO and Hg^0, the valence states of surface elements on the fresh and the used 2Fe4Co-MCT catalysts (after the removal of NO and Hg^0) were determined using XPS and the results are listed in Table 3. The fresh catalysts and the used catalysts after the experimental tests are denoted as "Fresh" and "Used", respectively. The "Used (SCR)" indicates the catalyst used in conventional SCR conditions, while the "Used (SCR+Hg)" indicates the catalyst used in SCR conditions where 35 μg m^{-3} Hg^0 was added.

Fig. 6(a) showed the O1s XPS spectra of the fresh and the used 2Fe4Co-MCT catalysts. Two overlapping peaks are observed in the fresh catalyst. However, a new peak at a higher binding energy appears in the used catalysts. The peaks appeared at binding energy (> 532.2 ev) in the used catalysts could be assigned to oxygen in hydroxyl species and/or surface adsorbed water (denoted as O_γ) [58-60]. The peaks at binding energy of 529.5–530.3 ev could be ascribed to lattice oxygen (denoted as O_β) in metal oxides [61, 62]. The peaks at around 531–532 ev cloud be attributed to surface

chemisorbed oxygen and/or weakly bonded oxygen species (donated as O_α), which played an important role in oxidation reactions [59, 60, 62]. The relative ratios of different oxygen species were calculated and listed in Table 3. It could be found that the ratio of O_β/O_α was increased in the "Used (SCR)" catalyst when compared to the fresh catalyst, demonstrating that the chemisorbed oxygen species after SCR reaction were decreased. Therefore, chemisorbed oxygen might play an important role on the conversion of NO in SCR. However, the ratio of O_β/O_α was decreased significantly in the "Used (SCR+Hg)" catalyst compared to the fresh catalyst, indicating that the decrease of lattice oxygen was greater than that of chemisorbed oxygen. This result was consistent with the results reported by Zhang et al [25] and He et al [58], indicating that the oxidation of Hg^0 was mainly attributed to the consumption of lattice oxygen in the catalysts.

The valence states of various metal elements before and after reactions were shown in Figs. 7(b)–(e). Two distinct peaks belonging to $Mn2p_{3/2}$ and $Mn2p_{1/2}$ could be seen for all the catalysts at binding energy around 642.4 and 654 ev (Fig. 6(b)), respectively. By peak-fitting deconvolution, the $Mn2p_{3/2}$ spectra were split into three peaks at binding energy of 641.2–641.8 ev, 642.2–643.4 ev and above 644 ev, which could be attributed to Mn^{3+}, Mn^{4+} and Mn-nitrate, respectively [47, 62, 63]. The presence of Mn-nitrate could be ascribed to the incomplete decomposition of manganese nitrate. The manganese oxides existed in the form of Mn_2O_3 and MnO_2 were the main active components of the catalyst for the removal of NO. The coexistence of MnO_2 and Mn_2O_3 is suggested to promote the oxidation of NO to NO_2, and improve the efficiency of NO

removal in the low-temperature SCR [47, 58, 62].

Ce3d XPS spectra are shown in Fig. 6(c). The $3d_{3/2}$ spin-orbit state is labeled with letters U. The $3d_{5/2}$ spin-orbit state is labeled with letters V. U'''(916.7 ev), U''(907.3 ev), U(901.0 ev), V'''(898.4 ev), V''(888.8 ev), V(882.5 ev) which are corresponded to Ce^{4+}. And U'(903.5 ev),V'(884.9 ev) are related to Ce^{3+} [64]. Ce^{4+} and Ce^{3+} were coexisted in the fresh and the used catalysts. CeO_2 has a cubic fluorite structure and typically possesses a relatively high density of oxygen vacancies [65], providing a higher oxidation state and intensified capacity of oxygen storage. Therefore, the oxidation of NO and Hg^0 was promoted in the presence of CeO_2. Ce^{3+} could create a charge imbalance, the vacancies and unsaturated chemical bonds on the surface of catalysts, which was helpful for the chemisorbed oxygen to be attached on the surface of catalyst [66, 67]. The presence of CeO_2 and Ce_2O_3 indicates that the redox shift between Ce^{4+} and Ce^{3+} could easily take place, promoting the removal of mercury [59].

Fig. 6(d) shows the XPS spectra of Fe2p in different catalyst samples. By peak-fitting deconvoluting, the peak at binding energy around 725 ev could be attributed to the $Fe2p_{1/2}$ spin-orbit [53]. The peak at binding energy of 710–711 ev could be ascribed to Fe^{2+} species, while the peak at about 711–712 ev could be assigned to Fe^{3+} species [60, 63]. The broad peak at around 719 ev indicates the presence of Fe^{3+}. Therefore, Fe^{2+} and Fe^{3+} coexisted on the surfaces of the catalysts [40, 60].

The fitted XPS spectra of $Co2p_{3/2}$ region for the fresh and the used catalysts are shown in Fig. 6(e). Three peaks could be observed in all samples. The peaks at binding energy of 780.0–781.0ev could be attributed to Co^{3+} [68], while the peaks at around 781.3–

782.6ev could be ascribed to Co^{2+} [43, 69]. The broad and gentle satellite structure at higher binding energy region could be ascribed to the shakeup process of Co^{2+} in the high spin state [69]. The results show that Co^{2+} and Co^{3+} were co-existed on the surfaces of the catalysts. It was reported that Co^{3+} species presented a relatively high oxidation state and resulted in more anionic defects, producing excess surface oxygen to facilitate the adsorption of gas molecular during NOx reduction reactions [69].

From Table 3, the ratio of Mn^{4+}/Mn^{3+} was similar between the fresh and the used catalysts. It has also been reported that the addition of CeO_2 maintained a higher Mn^{4+}/Mn^{3+} ratio through $2CeO_2 + Mn_2O_3 \rightarrow 2MnO_2 + Ce_2O_3$ [38, 47]. However, the ratios of Fe^{3+}/Fe^{2+} and Co^{3+}/Co^{2+} decreased after the experiments. In addition, the peaks assigned to Fe and Co cations shifted to higher binding energy region after the catalyst was used. It has been reported that the hydroxyl coordinated with metal cations was formed by metal species directly reacting with adsorbed NH_3 [70], which may be due to the shift to higher binding energy.

In the used (SCR+Hg) sample, the ratios of Ce^{4+}/Ce^{3+} and Co^{3+}/Co^{2+} all decreased apparently compared to the used (SCR) catalysts. Therefore, both Ce^{4+} and Co^{3+} played important roles in the oxidation of Hg^0. The ratio of Mn^{4+}/Mn^{3+} was slightly decreased in the used (SCR+Hg) sample. The change of Fe^{3+}/Fe^{2+} in the used (SCR+Hg) catalyst was small when compared to the used (SCR) sample. Furthermore, the ratio of Fe^{3+}/Fe^{2+} was significantly reduced in the SCR process. The results of XPS indicate that the introduction of Fe species in the catalyst enhanced the activity of SCR, whereas the introduction of Co species enhanced the oxidation of Hg^0. The synergistic effect of Fe

and Co species might play an important role for simultaneously removing NO and Hg^0. To identify the transformation of Hg^0 on the surface of the catalyst, XPS analysis of Hg4f was performed for the used (SCR+Hg) catalysts and the results are shown in Fig. 6(f). The peak at around 102.6–103.3 ev could be assigned to Si2p electron [59, 60], this might be due to that the reacted sample was mixed with quartz wool which was used to support the catalyst during the process. The small peaks at binding energy around 100.5–101.0 ev could be ascribed to HgO belonging to $Hg4f_{7/2}$. However, no peaks assigned to adsorbed Hg^0 (99.7–99.9 ev) was detected on the surface of the used catalyst. The concentration of Hg^0 on the surface of the sample could be lower than the detection limit of XPS analysis. Another possible reason could be that the physically adsorbed Hg^0 may have desorbed from the surface of the catalyst. The XPS results of Hg4f confirm that the oxidation of Hg^0 by oxygen species took place on the surface of the catalysts.

4. Conclusion

Fe and Co co-doped Mn-Ce/TiO_2 catalysts were investigated for the simultaneous removal of NO and Hg^0 at low temperatures. The results show that the 2Fe4Co-MCT catalyst exhibited the best performance for the simultaneous removal of NO and Hg^0 than the only Fe or Co doped catalysts. At low reaction temperature i.e. less than 200 °C, the adsorption of Hg^0 on the surface of catalyst was dominant compared to the adsorption of NO, benefiting the oxidation of Hg^0. However, when the reaction temperature was higher than 200 °C, NH_3 occupied most of the active sites on the surface of the catalyst, resulting in the reduction of the removal of Hg^0. Further

experimental tests and XPS analysis indicate that chemisorbed oxygen played a dominant role in SCR of NO, while lattice oxygen played a dominant role in Hg^0 oxidation. Additionally, the introduction of Fe species in the catalyst enhanced the activity of SCR whereas the introduction of Co species enhanced the oxidation of Hg^0.

Acknowledgments

The project was supported by the Natural Science Foundation of Hebei Province (E2016202361), Research Fund of International Young Scientists (51550110237) and State's Key Project of Research and Development Plan (2016YFC0209202).

References

[1] Z.-J. Zhou, X.-W. Liu, B. Zhao, Z.-G. Chen, H.-Z. Shao, L.-L. Wang, M.-H. Xu, Effects of existing energy saving and air pollution control devices on mercury removal in coal-fired power plants, Fuel Processing Technology, 131 (2015) 99-108.

[2] K.-M. Bae, B.-J. Kim, S.-J. Park, Overlook of carbonaceous adsorbents and processing methods for elemental mercury removal, Carbon letters, 15 (2014) 238-246.

[3] D. Pudasainee, J.-H. Kim, Y.-S. Yoon, Y.-C. Seo, Oxidation, reemission and mass distribution of mercury in bituminous coal-fired power plants with SCR, CS-ESP and wet FGD, Fuel, 93 (2012) 312-318.

[4] J. Ma, C. Li, L. Zhao, J. Zhang, J. Song, G. Zeng, X. Zhang, Y. Xie, Study on removal of elemental mercury from simulated flue gas over activated coke treated by acid, Applied Surface Science, 329 (2015) 292-300.

[5] H. Zeng, F. Jin, J. Guo, Removal of elemental mercury from coal combustion flue gas by chloride-impregnated activated carbon, Fuel, 83 (2004) 143-146.

[6] Z. Tan, L. Sun, J. Xiang, H. Zeng, Z. Liu, S. Hu, J. Qiu, Gas-phase elemental mercury removal by novel carbon-based sorbents, Carbon, 50 (2012) 362-371.

[7] Z. Tan, G. Niu, X. Chen, Removal of elemental mercury by modified bamboo carbon, Chinese Journal of Chemical Engineering, 23 (2015) 1875-1880.

[8] B. Shen, G. Li, F. Wang, Y. Wang, C. He, M. Zhang, S. Singh, Elemental mercury removal by the modified bio-char from medicinal residues, Chemical Engineering Journal, 272 (2015) 28-37.

[9] Y. Yao, V. Velpari, J. Economy, Design of sulfur treated activated carbon fibers for gas phase elemental mercury removal, Fuel, 116 (2014) 560-565.

[10] X.-y. Hua, J.-s. Zhou, Q. Li, Z.-y. Luo, K.-f. Cen, Gas-Phase Elemental Mercury Removal by CeO_2 Impregnated Activated Coke, Energy & Fuels, 24 (2010) 5426-5431.

[11] D. Musmarra, D. Karatza, A. Lancia, M. Prisciandaro, G. Mazziotti di Celso, Adsorption of elemental mercury vapors from synthetic exhaust combustion gas onto HGR carbon, Journal of the Air & Waste Management Association, 66 (2016) 698-706.

[12] P. Fang, C.-p. Cen, X.-m. Wang, Z.-j. Tang, Z.-x. Tang, D.-s. Chen, Simultaneous removal of SO_2, NO and Hg^0 by wet scrubbing using urea+$KMnO_4$ solution, Fuel Processing Technology, 106 (2013) 645-653.

[13] R.K. Nick D. Hutson, and Ravi K. Srivastava, Simultaneous Removal of SO_2, NO_X, and Hg from Coal Flue Gas Using a $NaClO_2$-Enhanced Wet Scrubber, Ind. Eng. Chem. Res., 47 (2008) 5825-5831.

[14] Z. Yi, J. Yao, X.-y. Ma, Absorption Behavior and Removal of Gaseous Elemental Mercury by Sodium Chlorite Solutions, Journal of Environmental Engineering, 138 (2012) 620-624.

[15] Y. Zhao, S.T. Liu, C.M. Chen, X.Y. Ma, Removal of Elemental Mercury by Sodium Chlorite Solution, Chemical Engineering & Technology, 31 (2008) 350-354.

[16] A.I. Martinez, B.K. Deshpande, Kinetic modeling of H_2O_2-enhanced oxidation of flue gas elemental mercury, Fuel Processing Technology, 88 (2007) 982-987.

[17] Y. Zhao, R. Hao, P. Zhang, S. Zhou, An integrative process for Hg_0 removal using vaporized H_2O_2/$Na_2S_2O_8$, Fuel, 136 (2014) 113-121.

[18] Y. Han, M. Fan, A.G. Russell, New insights into synergistic effects and active species toward Hg0 emission control by Fe(VI) absorbent, Fuel, 140 (2015) 309-316.

[19] D. Lu, E.J. Anthony, Y. Tan, R. Dureau, V. Ko, M.A. Douglas, Mercury removal from coal combustion by Fenton reactions – Part A: Bench-scale tests, Fuel, 86 (2007) 2789-2797.

[20] Y. Tan, D. Lu, E.J. Anthony, R. Dureau, R. Mortazavi, M.A. Douglas, Mercury removal from coal combustion by Fenton reactions. Paper B: Pilot-scale tests, Fuel, 86 (2007) 2798-2805.

[21] X. Weng, R. Mei, M. Shi, Q. Kong, Y. Liu, Z. Wu, $CePO_4$ Catalyst for Elemental Mercury Removal in Simulated Coal-Fired Flue Gas, Energy & Fuels, 29 (2015) 3359-3365.

[22] H. Xu, Z. Qu, C. Zong, F. Quan, J. Mei, N. Yan, Catalytic oxidation and adsorption of Hg0 over low-temperature NH_3-SCR $LaMnO_3$ perovskite oxide from flue gas, Applied Catalysis B: Environmental, 186 (2016) 30-40.

[23] Z. Zhou, X. Liu, B. Zhao, H. Shao, Y. Xu, M. Xu, Elemental mercury oxidation over manganese-based perovskite-type catalyst at low temperature, Chemical Engineering Journal, 288 (2016) 701-710.

[24] W. Chen, Y. Ma, N. Yan, Z. Qu, S. Yang, J. Xie, Y. Guo, L. Hu, J. Jia, The co-benefit of elemental mercury oxidation and slip ammonia abatement with SCR-Plus catalysts, Fuel, 133 (2014) 263-269.

[25] L. Qiu, J. Meng, D. Pang, C. Zhang, F. Ouyang, Reaction and Characterization of Co and Ce Doped Mn/TiO2 Catalysts for Low-Temperature SCR of NO with NH3, Catalysis Letters, 145 (2015) 1500-1509.

[26] A.G.-N.B. WOOJIN LEE Removal of Elemental Mercury ($Hg(^0)$) by Nanosized V_2O_5/TiO_2 Catalysts, Environ. Sci. Technol., 43 (2009) 1522-1527.

[27] H. Li, C.Y. Wu, Y. Li, L. Li, Y. Zhao, J. Zhang, Role of flue gas components in mercury oxidation over TiO_2 supported MnOx-CeO_2 mixed-oxide at low temperature, Journal of hazardous materials, 243 (2012) 117-123.

[28] G.K. Reddy, J. He, S.W. Thiel, N.G. Pinto, P.G. Smirniotis, Sulfur-Tolerant Mn-Ce-Ti Sorbents for Elemental Mercury Removal from Flue Gas: Mechanistic Investigation by XPS, The Journal of Physical Chemistry C, 119 (2015) 8634-8644.

[29] S. Zhang, Y. Zhao, Z. Wang, J. Zhang, L. Wang, C. Zheng, Integrated removal of

NO and mercury from coal combustion flue gas using manganese oxides supported on TiO2, Journal of Environmental Sciences, 53 (2017) 141-150.

[30] S. Zhang, Y. Zhao, J. Yang, Y. Zhang, P. Sun, X. Yu, J. Zhang, C. Zheng, Simultaneous NO and mercury removal over $MnOx/TiO_2$ catalyst in different atmospheres, Fuel Processing Technology, 166 (2017) 282-290.

[31] U. Bentrup, A. Brückner, M. Richter, R. Fricke, NOx adsorption on MnO2/NaY composite: an in situ FTIR and EPR study, Applied Catalysis B: Environmental, 32 (2001) 229-241.

[32] P.G. Smirniotis, D.A. Pena, B.S. Uphade, Low-temperature selective catalytic reduction (SCR) of NO with NH_3 by using Mn, Cr, and Cu oxides supported on Hombikat TiO_2, Angewandte Chemie-International Edition, 40 (2001) 2479-2482.

[33] G. Marbán, T. Valdés-Solís, A.B. Fuertes, Mechanism of low-temperature selective catalytic reduction of NO with NH_3 over carbon-supported Mn_3O_4: Role of surface NH3 species: SCR mechanism, Journal of Catalysis, 226 (2004) 138-155.

[34] L. Ji, P.M. Sreekanth, P.G. Smirniotis, S.W. Thiel, N.G. Pinto, Manganese oxide/titania materials for removal of NOx and elemental mercury from flue gas, Energy & Fuels, 22 (2008) 2299-2306.

[35] F.ç. Larachi, J. Pierre, A. Adnot, A. Bernis, Ce 3d XPS study of composite $CexMn1{-}xO_2{-}y$ wet oxidation catalysts, Applied Surface Science, 195 (2002) 236-250.

[36] B. Shen, F. Wang, T. Liu, Homogeneous MnOx–CeO2 pellets prepared by a one-step hydrolysis process for low-temperature NH3-SCR, Powder Technology, 253 (2014) 152-157.

[37] B. Shen, Y. Wang, F. Wang, T. Liu, The effect of Ce–Zr on NH_3-SCR activity over $MnOx(0.6)/Ce_{0.5}Zr_{0.5}O_2$ at low temperature, Chemical Engineering Journal, 236 (2014) 171-180.

[38] G. Qi, R.T. Yang, R. Chang, $MnOx\text{-}CeO_2$ mixed oxides prepared by co-precipitation for selective catalytic reduction of NO with NH_3 at low temperatures, Applied Catalysis B: Environmental, 51 (2004) 93-106.

[39] G. Qi, R.T. Yang, Low-temperature selective catalytic reduction of NO with NH_3 over iron and manganese oxides supported on titania, Applied Catalysis B:

Environmental, 44 (2003) 217-225.

[40] B. Shen, T. Liu, N. Zhao, X. Yang, L. Deng, Iron-doped Mn-Ce/TiO_2 catalyst for low temperature selective catalytic reduction of NO with NH_3, Journal of Environmental Sciences, 22 (2010) 1447-1454.

[41] K. Góra-Marek, K. Brylewska, K.A. Tarach, M. Rutkowska, M. Jabłońska, M. Choi, L. Chmielarz, IR studies of Fe modified ZSM-5 zeolites of diverse mesopore topologies in the terms of their catalytic performance in NH_3-SCR and NH_3-SCO processes, Applied Catalysis B: Environmental, 179 (2015) 589-598.

[42] M. Qiu, S. Zhan, H. Yu, D. Zhu, Low-temperature selective catalytic reduction of NO with NH3 over ordered mesoporous $MnxCo_3 - xO_4$ catalyst, Catalysis Communications, 62 (2015) 107-111.

[43] D. Shang, Q. Zhong, W. Cai, High performance of NO oxidation over Ce–Co–Ti catalyst: The interaction between Ce and Co, Applied Surface Science, 325 (2015) 211-216.

[44] S.C. Petitto, E.M. Marsh, G.A. Carson, M.A. Langell, Cobalt oxide surface chemistry: The interaction of CoO(1 0 0), Co_3O_4(1 1 0) and Co_3O_4(1 1 1) with oxygen and water, Journal of Molecular Catalysis A: Chemical, 281 (2008) 49-58.

[45] C. Wang, D. Zhou, Z. Chen, T. Gao, S. Naito, Enhanced Catalytic Reduction of NO by H2 over Nanoporous Nickel Phosphate VSB-5-Type Catalysts, Bulletin of the Chemical Society of Japan, 88 (2015) 1431-1436.

[46] D. Gao, Q. Gao, Selective oxidation of styrene to benzaldehyde over VSB-5 and isomorphously substituted cobalt VSB-5, Catalysis Communications, 8 (2007) 681-685.

[47] Y. Wang, B. Shen, C. He, S. Yue, F. Wang, Simultaneous Removal of NO and Hg(0) from Flue Gas over Mn-Ce/Ti-PILCs, Environmental science & technology, 49 (2015) 9355-9363.

[48] H. Li, C.-Y. Wu, Y. Li, J. Zhang, Superior activity of MnOx-CeO_2/TiO_2 catalyst for catalytic oxidation of elemental mercury at low flue gas temperatures, Applied Catalysis B: Environmental, 111-112 (2012) 381-388.

[49] P. Wang, S. Su, J. Xiang, F. Cao, L. Sun, S. Hu, S. Lei, Catalytic oxidation of Hg^0 by CuO–MnO_2–Fe_2O_3/γ-Al_2O_3 catalyst, Chemical Engineering Journal, 225 (2013) 68-

75.

[50] X. Li, J. Li, Y. Peng, H. Chang, T. Zhang, S. Zhao, W. Si, J. Hao, Mechanism of arsenic poisoning on SCR catalyst of CeW/Ti and its novel efficient regeneration method with hydrogen, Applied Catalysis B: Environmental, 184 (2016) 246-257.

[51] J. Li, C. Yang, Q. Zhang, Z. Li, W. Huang, Effects of Fe addition on the structure and catalytic performance of mesoporous Mn/Al–SBA-15 catalysts for the reduction of NO with ammonia, Catalysis Communications, 62 (2015) 24-28.

[52] S.S.R. Putluru, L. Schill, A.D. Jensen, B. Siret, F. Tabaries, R. Fehrmann, Mn/TiO_2 and $Mn–Fe/TiO_2$ catalysts synthesized by deposition precipitation—promising for selective catalytic reduction of NO with NH_3 at low temperatures, Applied Catalysis B: Environmental, 165 (2015) 628-635.

[53] F. Liu, H. He, C. Zhang, Z. Feng, L. Zheng, Y. Xie, T. Hu, Selective catalytic reduction of NO with NH_3 over iron titanate catalyst: Catalytic performance and characterization, Applied Catalysis B: Environmental, 96 (2010) 408-420.

[54] A. Khan, P.G. Smirniotis, Relationship between temperature-programmed reduction profile and activity of modified ferrite-based catalysts for WGS reaction, Journal of Molecular Catalysis A: Chemical, 280 (2008) 43-51.

[55] F. Cao, S. Su, J. Xiang, P. Wang, S. Hu, L. Sun, A. Zhang, The activity and mechanism study of $Fe–Mn–Ce/\gamma\text{-}Al_2O_3$ catalyst for low temperature selective catalytic reduction of NO with NH_3, Fuel, 139 (2015) 232-239.

[56] M. Qiu, S. Zhan, H. Yu, D. Zhu, Low-temperature selective catalytic reduction of NO with NH_3 over ordered mesoporous $MnxCo_3{-}xO_4$ catalyst, Catalysis Communications, 62 (2015) 107-111.

[57] C. Shi, Y. Wang, A. Zhu, B. Chen, C. Au, $MnxCo_3{-}xO_4$ solid solution as high-efficient catalysts for low-temperature oxidation of formaldehyde, Catalysis Communications, 28 (2012) 18-22.

[58] C. He, B. Shen, J. Chen, J. Cai, Adsorption and oxidation of elemental mercury over Ce-MnOx/Ti-PILCs, Environmental science & technology, 48 (2014) 7891-7898.

[59] S. Tao, C. Li, X. Fan, G. Zeng, P. Lu, X. Zhang, Q. Wen, W. Zhao, D. Luo, C. Fan, Activated coke impregnated with cerium chloride used for elemental mercury removal

from simulated flue gas, Chemical Engineering Journal, 210 (2012) 547-556.

[60] Y. Wang, C. Li, L. Zhao, Y. Xie, X. Zhang, G. Zeng, H. Wu, J. Zhang, Study on the removal of elemental mercury from simulated flue gas by Fe_2O_3-CeO_2/AC at low temperature, Environmental science and pollution research international, 23 (2016) 5099-5110.

[61] F. Wang, G. Li, B. Shen, Y. Wang, C. He, Mercury removal over the vanadia–titania catalyst in CO_2-enriched conditions, Chemical Engineering Journal, 263 (2015) 356-363.

[62] L. Zhao, C. Li, X. Zhang, G. Zeng, J. Zhang, Y. Xie, Oxidation of elemental mercury by modified spent TiO_2-based SCR-DeNOx catalysts in simulated coal-fired flue gas, Environmental science and pollution research international, 23 (2016) 1471-1481.

[63] J. Li, J. Chen, Y. Yu, C. He, Fe–Mn–Ce/ceramic powder composite catalyst for highly volatile elemental mercury removal in simulated coal-fired flue gas, Journal of Industrial and Engineering Chemistry, 25 (2015) 352-358.

[64] P. Patsalas, S. Logothetidis, L. Sygellou, S. Kennou, Structure-dependent electronic properties of nanocrystalline cerium oxide films, Physical Review B, 68 (2003) 1-12.

[65] X. Fan, C. Li, G. Zeng, X. Zhang, S. Tao, P. Lu, Y. Tan, D. Luo, Hg^0 Removal from Simulated Flue Gas over CeO_2/HZSM-5, Energy & Fuels, 26 (2012) 2082-2089.

[66] S. Yang, W. Zhu, Z. Jiang, Z. Chen, J. Wang, The surface properties and the activities in catalytic wet air oxidation over CeO_2–TiO_2 catalysts, Applied Surface Science, 252 (2006) 8499-8505.

[67] X. Gao, Y. Jiang, Y. Zhong, Z. Luo, K. Cen, The activity and characterization of CeO_2-TiO_2 catalysts prepared by the sol-gel method for selective catalytic reduction of NO with NH_3, Journal of hazardous materials, 174 (2010) 734-739.

[68] X. Tang, F. Gao, Y. Xiang, H. Yi, S. Zhao, Low temperature catalytic oxidation of nitric oxide over the Mn–CoOx catalyst modified by nonthermal plasma, Catalysis Communications, 64 (2015) 12-17.

[69] H. Hu, S. Cai, H. Li, L. Huang, L. Shi, D. Zhang, Mechanistic Aspects of

deNOxProcessing over TiO_2 Supported Co–Mn Oxide Catalysts: Structure–Activity Relationships and In Situ DRIFTs Analysis, ACS Catalysis, 5 (2015) 6069-6077.

[70] S. Yang, Y. Liao, S. Xiong, F. Qi, H. Dang, X. Xiao, J. Li, N_2 Selectivity of NO Reduction by NH_3 over MnOx–CeO_2: Mechanism and Key Factors, The Journal of Physical Chemistry C, 118 (2014) 21500-21508.

Table 1

Experimental conditions using different MCT based catalysts

Experiments	Catalysts	Gas Atmosphere (Total flow rate = 1500 mL min^{-1})	Temperature （°C）
Set A	6Co-MCT，6Fe-MCT，2Fe4Co-MCT	N_2 + 5% O_2 + 500 ppm NO + 500 ppm NH_3 + 35 μg m^{-3} Hg^0	100–300
Set B	2Fe4Co-MCT	N_2 + 5% O_2 + 500 ppm NO + 500 ppm NH_3 N_2 + 5% O_2 + 500 ppm NO + 500 ppm NH_3 + 35 μg m^{-3} Hg^0	100–300
Set C	2Fe4Co-MCT	N_2 + 5% O_2 + 35 μg m^{-3} Hg^0 N_2 + 5% O_2 + 500 ppm NO + 500 ppm NH_3 + 35 μg m^{-3} Hg^0	100–300
Set D	2Fe4Co-MCT	N_2 + 35 μg m^{-3} Hg^0 N_2 + 5% O_2 + 35 μg m^{-3} Hg^0 N_2 + 5% O_2 + 500 ppm NO + 35 μg m^{-3} Hg^0 N_2 + 5% O_2 + 500 ppm NH_3 + 35 μg m^{-3} Hg^0 N_2 + 5% O_2 + 500 ppm NO + 500 ppm NH_3 + 35 μg m^{-3} Hg^0	200

Table 2

Physical characteristics of selected catalysts

Catalysts	BET surface area (m^2 g^{-1})	Pore volume (cm^3 g^{-1})	Pore size (nm)
Mn-Ce/TiO_2	17.06	0.029	6.90
6Fe-Mn-Ce/TiO_2	22.25	0.048	8.71
6Co-Mn-Ce/TiO2	16.37	0.032	7.83
2Fe4Co-Mn-Ce/TiO_2	23.02	0.044	7.62

Table 3

Relative concentration ratios of different catalysts

Samples	Relative concentration ratios						
	Mn^{4+}/Mn^{3+}	Ce^{4+}/Ce^{3+}	Fe^{3+}/Fe^{2+}	Co^{3+}/Co^{2+}	O_α/O_T	O_β/O_T	O_β/O_α
Fresh	0.88	4.3	1.42	1.68	0.44	0.56	1.27
Used (SCR)	0.87	4.32	1.18	1.56	0.24	0.46	1.91
Used (SCR + Hg)	0.81	4.04	1.2	1.09	0.41	0.29	0.70

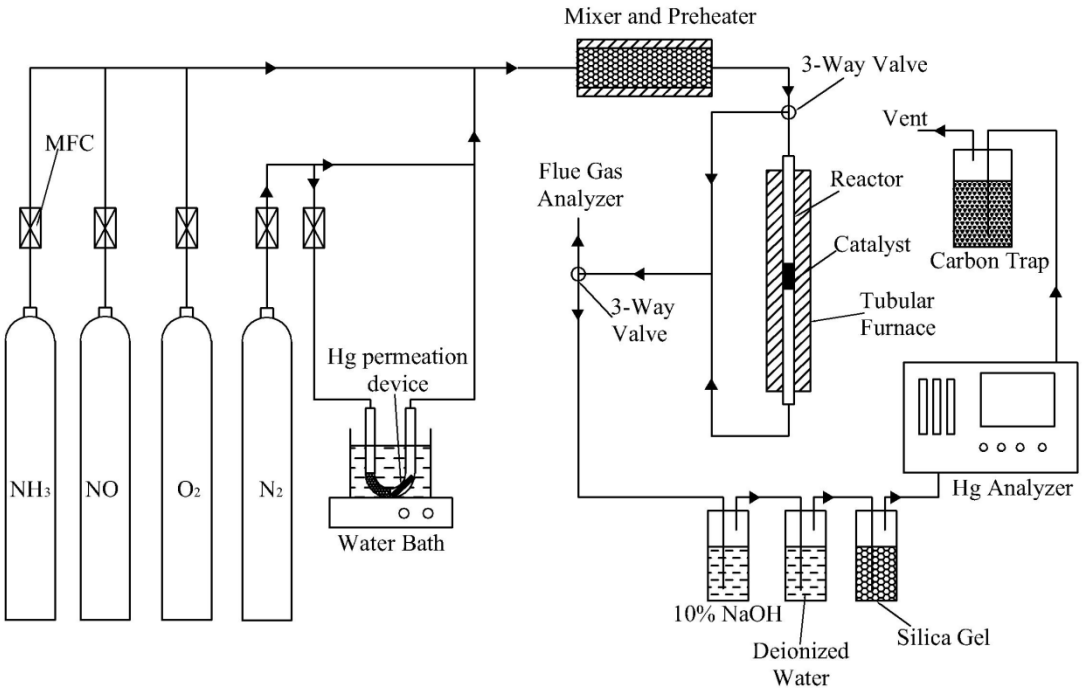

Figure 1 Schematic diagram of experimental system set-up

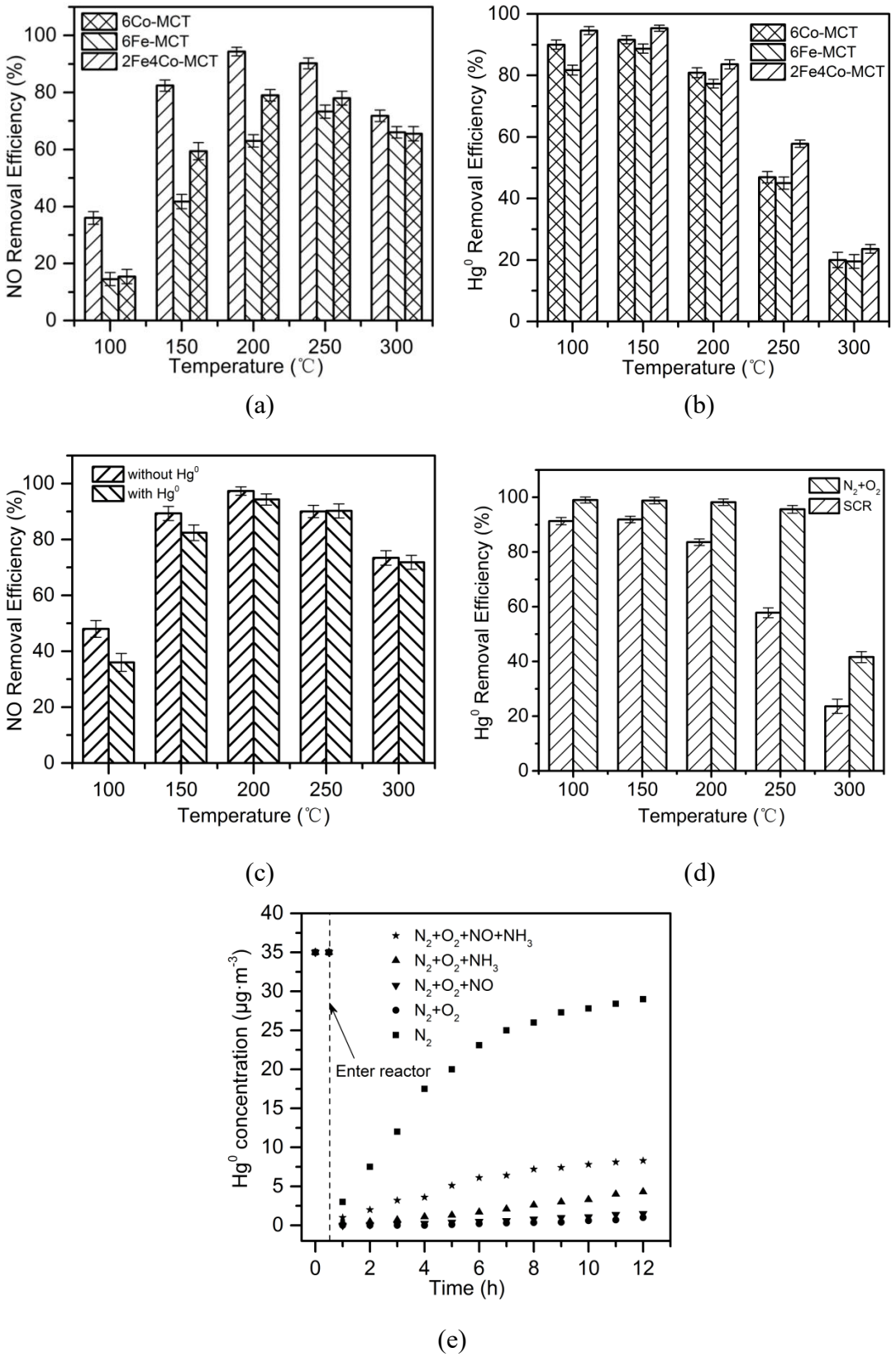

Figure 2 Effect of (a) NO removal efficiency; (b) Hg^0 removal efficiency; (c) Hg^0 on NO removal efficiency; (d) SCR conditions on Hg^0 removal efficiency and (e) Flue gas components on Hg^0 removal on the simultaneous removal of NO and Hg^0 using different catalysts

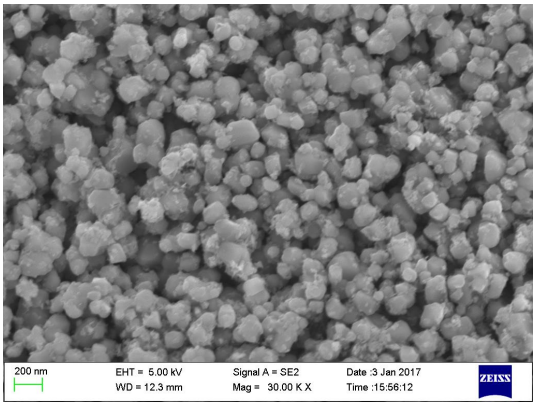

(a) 2Fe4Co-MCT

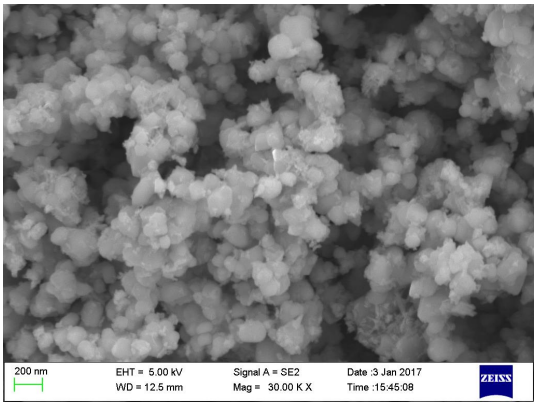

(b) 6Co-MCT

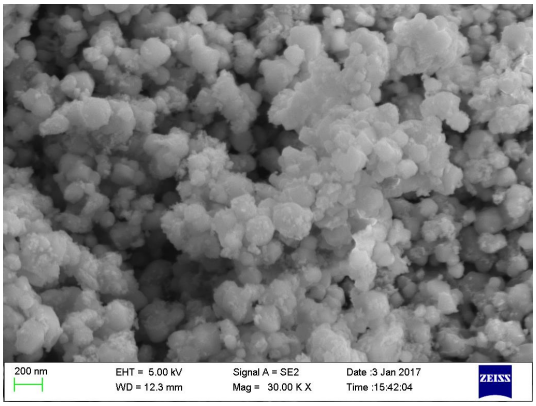

(c) 6Fe-MCT

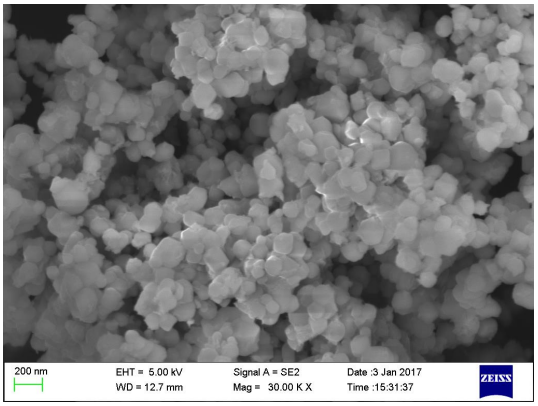

(d) MCT

Figure 3 SEMs results of MCT, 6Fe-MCT, 6Co-MCT, 2Fe4Co-MCT

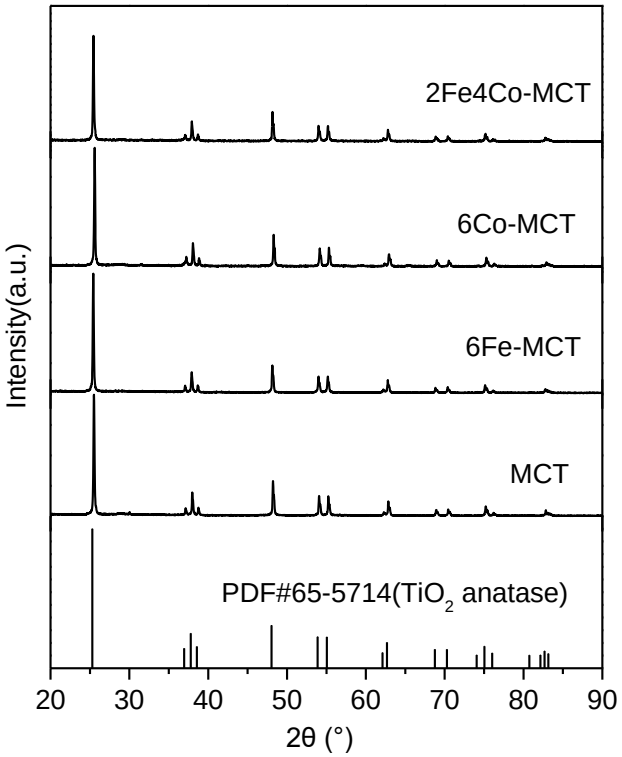

Figure 4 XRD results of MCT, 6Fe-MCT, 6Co-MCT and 2Fe4Co-MCT catalysts

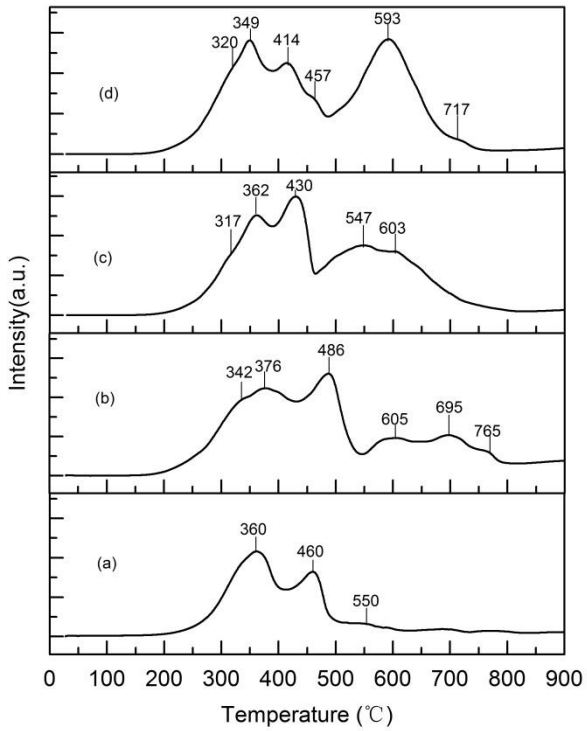

Figure 5 H_2-TPR of (a) Mn-Ce/TiO_2, (b) 6Fe-Mn-Ce/TiO_2, (c) 6Co-Mn-Ce/TiO_2 and (d) 2Fe4Co-Mn-Ce/TiO_2 catalysts

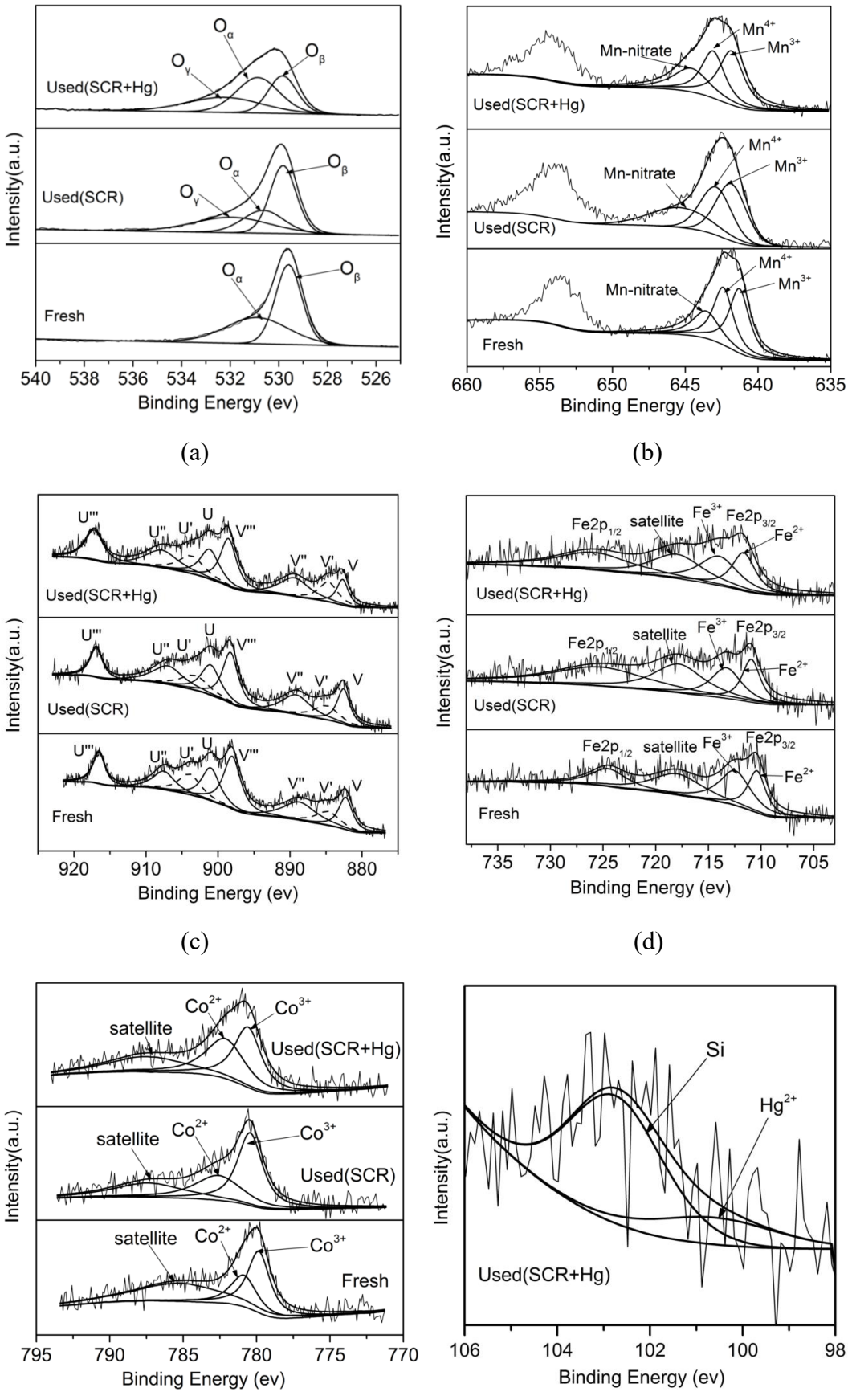

Figure 6 XPS spectra of different samples. (a) O1s; (b) Mn2p; (c) Ce3d; (d) Fe2p; (e) Co2p and (f) Hg4f